Inorg. Chem. **2009**, *48*, 652–662

Inorganic Chemistry
Article

Transformations and Reactions of $Re_2(CO)_8(\mu\text{-}SbPh_2)(\mu\text{-}H)$ Induced by the Addition of a Platinum(tri-*t*-butylphosphine) Group

Richard D. Adams,*,† Michael B. Hall,*,‡ William C. Pearl, Jr.,† and Xinzheng Yang‡

Department of Chemistry and Biochemistry, University of South Carolina, Columbia, South Carolina 29208, and Department of Chemistry, Texas A&M University, College Station, Texas 77843-3255

Received October 3, 2008

Three products $Re_2[Pt(PBu^t_3)](\mu\text{-}SbPh_2)(CO)_8(\mu\text{-}H)$, **2**, $Re_2[Pt(CO)(PBu^t_3)]Ph(CO)_8(\mu_3\text{-}SbPh)(\mu\text{-}H)$, **3**, and $Re_2[Pt(PBu^t_3)]_2(CO)_8(\mu_4\text{-}Sb_2Ph_2)(\mu\text{-}H)_2$, **4**, were obtained from the reaction of $Re_2(CO)_8(\mu\text{-}SbPh_2)(\mu\text{-}H)$, **1**, with $Pt(PBu^t_3)_2$. Compound **3** was also obtained from **2** by further reaction with $Pt(PBu^t_3)_2$. Compound **2** is a $Pt(PBu^t_3)$ adduct of **1** formed by the insertion of the platinum atom into one of the Re−Sb bonds of **1** with formation of two Pt−Re bonds. Compound **3** contains an open Re_2Pt cluster and was also obtained in a low yield by the addition of CO to **2**. The addition of $SbPh_3$ to **2** yielded the compound $Re_2Pt(PBu^t_3)(Ph)(CO)_8(SbPh_3)(\mu_3\text{-}SbPh)(\mu\text{-}H)$, **5**, a $SbPh_3$ derivative of **3**. Compound **4** can be viewed as a dimer of the fragment $Re[Pt(PBu^t_3)](CO)_4(SbPh)(\mu\text{-}H)$. The two halves of the molecule are held together by Pt−Sb bonds and a significant interaction directly between the Sb atoms, Sb−Sb distance, 2.9834(7) Å. The Sb−Sb bonding in **4** was explained by density functional calculations. Compound **4** adds 2 equiv of CO at 1 atm/25 °C, one to each platinum atom, to yield the compound $[Re(CO)_4Pt(H)(CO)(PBu^t_3)(\mu_3\text{-}SbPh)]_2$ which exists as a mixture of two noninterconverting isomers, cis-**6** and trans-**6.** Both isomers of **6** were isolated and structurally characterized. Each isomer of **6** consists of a central planar Re_2Sb_2 core composed of two $Re(CO)_4$ groups with two bridging SbPh ligands. There is a $Pt(H)(CO)(PBu^t_3)$ group coordinated to each antimony atom of **6**. In the cis-isomer both $Pt(H)(CO)(PBu^t_3)$ groups lie on the same side of the Re_2Sb_2 plane. In the trans-isomer the $Pt(H)(CO)(PBu^t_3)$ groups lie on opposite sides of the Re_2Sb_2 plane.

Introduction

Studies have shown that the introduction of bulky phosphine ligands into polynuclear metal cluster complexes often produces electronic unsaturation at the metal atoms by forcing out ligands that would ordinarily occupy sites on those metal atoms. It has been found that this electronic unsaturation can lead to enhanced reactivity toward the very small molecule hydrogen.[1] We have recently shown that the compounds $M(PBu^t_3)_2$, M = Pd or Pt are excellent reagents for the addition of $M(PBu^t_3)$ groups to the metal−metal bonds of transition metal carbonyl cluster complexes.[2−6] For example, the reactions of $Ru_3(CO)_{12}$ with $Pd(PBu^t_3)_2$ and $Pt(PBu^t_3)_2$ yielded the tris-$M(PBu^t_3)$ adducts, $Ru_3(CO)_{12}[M(PBu^t_3)]_3$, M = Pd and Pt. Both compounds contain a $M(PBu^t_3)$ group bridging each of the three Ru−Ru bonds of the original molecule of $Ru_3(CO)_{12}$, eq 1.[2,3]

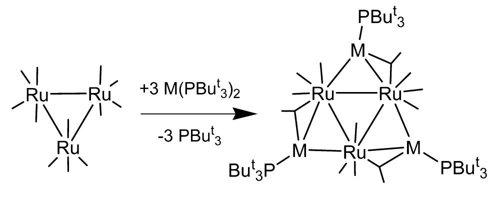

(1)

M = Pd or Pt

We have found that some of these new unsaturated mixed metal complexes containing $Pt(PBu^t_3)$ groupings readily activate hydrogen under mild conditions.[6] For example, $Re_2Pt_3(CO)_6(PBu^t_3)_3$ sequentially adds 3 equiv of H_2 at room temperature, eq 2.[6a]

* To whom correspondence should be addressed. E-mail: adams@mail.chem.sc.edu.
† University of South Carolina.
‡ Texas A&M University.

(1) (a) Weller, A. S.; McIndoe, J. S. *Eur. J. Inorg. Chem.* **2007**, 4411–4423. (b) Adams, R. D.; Captain, B. *Angew. Chem., Int. Ed.* **2008**, *47*, 252–257.
(2) Adams, R. D.; Captain, B.; Fu, W.; Hall, M. B.; Manson, J.; Smith, M. D.; Webster, C. E. *J. Am. Chem. Soc.* **2004**, *126*, 5253–5267.

10.1021/ic801876s CCC: $40.75

Published on Web 12/10/2008

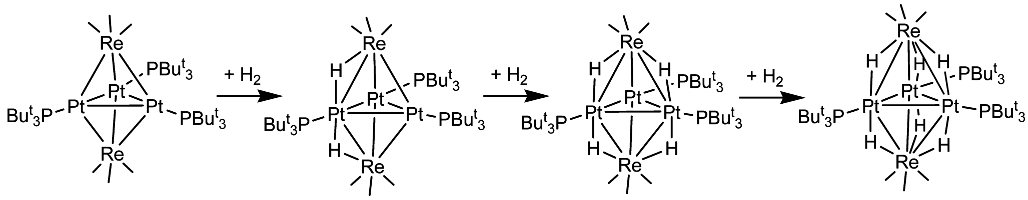

(2)

We have found that it is also possible to add $Pd(PBu^t_3)$ and $Pt(PBu^t_3)$ groups to transition metal−tin bonds. The reaction of $Pt(PBu^t_3)_2$ with $Ru_3(CO)_9(\mu\text{-}SnPh_2)_3$ yielded the product $Ru_3(CO)_9(\mu\text{-}SnPh_2)_3[Pt(PBu^t_3)]_3$, eq 3.[7] The reaction of the $Re_2(CO)_8(\mu\text{-}SnPh_2)_2$ with $Pd(PBu^t_3)_2$ and $Pt(PBu^t_3)_2$ yielded the compounds $Re_2(CO)_8(\mu\text{-}SnPh_2)_2[M(PBu^t_3)]_2$, M = Pd and Pt, eq 4.[8]

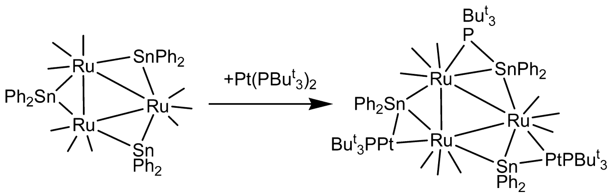

(3)

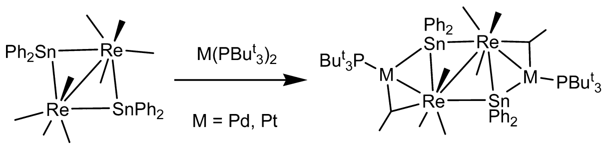

(4)

In the reaction of $Ru_2(CO)_8(\mu\text{-}SnPh_2)$ with $Pt(PBu^t_3)_2$, the Ru−Ru bond was metalated first by $Pt(PBu^t_3)$ to yield $Ru_2(CO)_8(\mu\text{-}SnPh_2)[Pt(PBu^t_3)]$; however, a second $Pt(PBu^t_3)$ addition yielded the bis-$Pt(PBu^t_3)$ adduct, $Ru_2(CO)_8(\mu\text{-}SnPh_2)[Pt(PBu^t_3)]_2$, by platinum addition to one of the Ru−Sn bonds eq 5.[9]

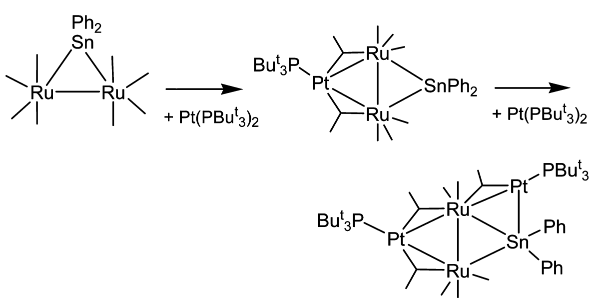

(5)

When the metal−metal bond contains a bridging hydrido ligand, the $Pt(PBu^t_3)$ group may be inserted into the metal−metal bond. For example, the reaction of $Pt(PBu^t_3)_2$ with $Re_3(CO)_{12}(\mu\text{-}H)_3$ with $Pt(PBu^t_3)_2$ yielded the mono-$Pt(PBu^t_3)$ adduct, $Re_3(CO)_{12}(\mu\text{-}H)_3[Pt(PBu^t_3)]$, eq 6.[6a]

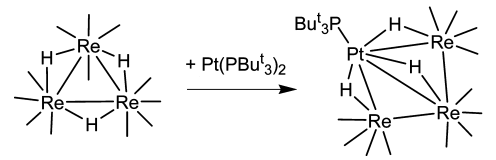

(6)

It has also been found that the M−H bond of the tin-containing mononuclear metal carbonyl hydride complexes $HM(CO)_4SnPh_3$, M = Ru, Os, is activated toward insertion of HC_2Ph when $Pd(PBu^t_3)$ and $Pt(PBu^t_3)$ groups are added to them, for example, eq 7.[10]

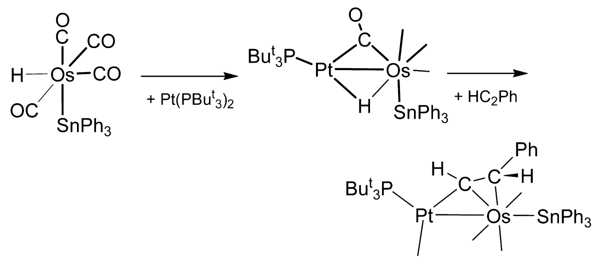

(7)

To expand our studies of the versatile reactivity and bonding capabilities of the $Pt(PBu^t_3)$ group, we have now investigated the reaction of the compound $Re_2(CO)_8(\mu\text{-}SbPh_2)(\mu\text{-}H)$, **1** with $Pt(PBu^t_3)_2$. Compound **1** is structurally very similar to $Ru_2(CO)_8(\mu\text{-}SnPh_2)$, eq 5, except that it contains a bridging hydrido ligand across its metal−metal bond.[11] The results of our study of this reaction and the characterization of the products are described in this report.

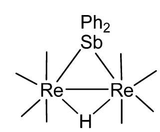

1

Experimental Section

General Data. Reagent grade solvents were dried by the standard procedures and were freshly distilled prior to use. Infrared spectra were recorded on a Thermo Nicolet Avatar 360 FT-IR spectrophotometer. ^1H NMR and $^{31}P\{^1H\}$ NMR were recorded on a Varian Mercury 400 spectrometer operating at 400.1 and 161.9 MHz,

(3) Adams, R. D.; Boswell, E. M.; Captain, B.; Zhu, L. *J. Cluster Sci.* **2008**, *19*, 121–132.
(4) (a) Adams, R. D.; Captain, B.; Smith, M. D.; Zhu, L. *Inorg. Chem.* **2006**, *45*, 430–436. (b) Adams, R. D.; Captain, B.; Zhu, L. *J. Cluster Sci.* **2006**, *17*, 87–95.
(5) Adams, R. D.; Captain, B.; Smith, M. D. *J. Cluster Sci.* **2004**, *15*, 139–149.
(6) (a) Adams, R. D.; Captain, B.; Smith, M. D.; Beddie, C.; Hall, M. B. *J. Am. Chem. Soc.* **2007**, *129*, 5981–5991. (b) Adams, R. D.; Captain, B.; Beddie, C.; Hall, M. B. *J. Am. Chem. Soc.* **2007**, *129*, 986–1000. (c) Adams, R. D.; Captain, B.; Zhu, L. *J. Organomet. Chem.* **2008**, *693*, 816–833. (d) Adams, R. D.; Boswell, E. M.; Hall, M. B.; Yang, X. *Organometallics* **2008**, *27*, 4938–4947.
(7) Adams, R. D.; Captain, B.; Hall, M. B.; Trufan, E.; Yang, X. *J. Am. Chem. Soc.* **2007**, *129*, 12328–12340.
(8) Adams, R. D.; Captain, B.; Herber, R. H.; Johansson, M.; Nowik, I., Jr.; Smith, M. D. *Inorg. Chem.* **2005**, *44*, 6346–6358.
(9) Adams, R. D.; Trufan, E. *Organometallics* **2008**, *27*, 4108–4115.
(10) (a) Adams, R. D.; Captain, B.; Trufan, E.; Zhu, L. *J. Am. Chem. Soc.* **2007**, *129*, 7545–7556. (b) Adams, R. D.; Captain, B.; Zhu, L. *J. Am. Chem. Soc.* **2006**, *128*, 13672–13673.
(11) Adams, R. D.; Captain, B.; Pearl, W. C., Jr. *J. Organomet. Chem.* **2008**, *693*, 1636–1644.

respectively. $^{31}P\{^1H\}$ NMR spectra were externally referenced against 85% *ortho*-H_3PO_4. Mass spectrometric measurements were performed on a VG 70S instrument by using a direct exposure probe and electron impact ionization (EI). $Pt(PBu^t_3)_2$, $SbPh_3$, and $Re_2(CO)_{10}$ were obtained from STREM and were used without further purification. $Re_2(CO)_8(\mu\text{-}SbPh_2)(\mu\text{-}H)$, **1**, was prepared as previously described.[11] Product separations were performed by TLC in air on Analtech 0.25 and 0.50 mm silica gel 60 Å F_{254} glass plates. Elemental analyses were performed by Desert Analytics (Tucson, AZ).

Reaction of $Re_2(CO)_8(\mu\text{-}SbPh_2)(\mu\text{-}H)$, 1 and $Pt(PBu^t_3)_2$. $Pt(PBu^t_3)_2$ (98.6 mg, 0.165 mmol) was added to a suspension of **1** (76.1 mg, 0.0871 mmol) in 20 mL of freshly distilled hexane and heated to hexane reflux for 1.5 h after which the solvent was removed in vacuo. The residue was extracted in methylene chloride and separated by TLC by using 4:1 hexane/methylene chloride (v/v) solvent mixture to give the following products in order of elution: a colorless band of unreacted **1** (28.3 mg, 37%), a violet band of $Re_2[Pt(PBu^t_3)]_2(CO)_8(\mu_4\text{-}Sb_2Ph_2)(\mu\text{-}H)_2$, **4** (2.1 mg, 1%), an orange band of $Re_2Pt(PBu^t_3)(CO)_8(\mu\text{-}SbPh_2)(\mu\text{-}H)$, **2** (7.1 mg, 39%), and a yellow band of $Re_2[Pt(CO)(PBu^t_3)]Ph(CO)_8(\mu_3\text{-}SbPh)(\mu\text{-}H)$, **3** (6.0 mg, 4%). Spectral data for **2**: IR (ν_{CO} cm^{-1} in hexane): 2071(w), 2037(w), 1988(s), 1963(w), 1959(w), 1929(w) cm^{-1}. ^1H NMR [CD_2Cl_2] $\delta = 7.83-7.08$ (m, Ph, 10H), 1.36 (d, CH_3, 27H, $^2J_{P-H}$ =13 Hz), −8.00 (d, hydride, 1H, $^1J_{195Pt-H} = 990$ Hz, $^2J_{P-H} = 10$ Hz); ^{31}P NMR [CD_2Cl_2] $\delta = 124.21$ (s, P, $^1J_{195Pt-P} = 3735$ Hz) ppm. Elemental analysis (%) calcd: 30.24, C; 3.01, H. Found 30.39, C; 3.17, H. Spectral data for **3**: IR (ν_{CO} cm^{-1} in hexane): 2090(w), 2073(m), 2054(w), 2009(w), 1999(s), 1982(m), 1974(w), 1960(s), 1942(w), 1930(w) cm^{-1}. NMR [CD_2Cl_2] $\delta = 7.97-6.90$ (m, Ph, 10H), 1.57 (d, CH_3, 27H, $^3J_{P-H} = 13$ Hz), −8.02 (d, hydride, 1H, $^2J_{P-H} = 13$ Hz, $^1J_{195Pt-H} = 552$ Hz); ^{31}P NMR [CD_2Cl_2] $\delta = 82.98$ (s, P, $^1J_{195Pt-P} = 2749$ Hz). Mass Spec. EI/MS *m/z*. 1298. The isotope pattern is consistent with the presence of two rhenium atoms, one antimony atom and one platinum atom. Spectral data for **4**: IR (ν_{CO} cm^{-1} in hexane): 2080(w), 2067(m), 1993(w), 1976(s), 1943(s) cm^{-1}. ^1H NMR [CD_2Cl_2] $\delta = 7.15-6.71$ (m, Ph, 10H), −8.27 (s, hydride, 2H, $^1J_{Pt-H} = 708$ Hz, $^2J_{P-H} = 10$ Hz), 1.66 (d, CH_3, 54H, $^2J_{P-H} = 12$ Hz); ^{31}P NMR [CD_2Cl_2] $\delta = 91.80$ (d, P, $^1J_{195Pt-H} = 3654$, $^3J_{195Pt-H} = 25.762$, $^4J_{P-P} = 32$ Hz). Mass Spec. EI/MS *m/z* = 1790, parent ion. The isotope pattern is consistent with the presence of two rhenium, two antimony, and two platinum atoms.

Thermal Decomposition of 2. 18.4 mg of **2** was dissolved in 20 mL of freshly distilled octane and heated to reflux for 30 min. The solvent was then removed in vacuo, and the residue was extracted in methylene chloride and separated by TLC by using 3:1 hexane/methylene chloride (v/v) solvent mixture to give the following products in order of elution: a colorless band of **1** (6.6 mg, 52%), a trace of recovered **2** (0.2 mg, 1%), and a yellow band of **3** (1.8 mg, 10%).

Reaction of 2 and $Pt(PBu^t_3)_2$. $Pt(PBu^t_3)_2$ (27.5 mg, 0.0459 mmol) was added to a suspension of **2** (27.3 mg, 0.0215 mmol) in 20 mL of freshly distilled hexane and heated to hexane reflux for 2 h. The solvent was removed in vacuo, and the residue was extracted in methylene chloride and separated by TLC by using a 4:1 hexane/methylene chloride (v/v) solvent mixture to give the following products in order of elution: a colorless band of **1** (1.7 mg, 9%), purple **4** (1.0 mg, yield 5%), orange **2** (8.4 mg, 31%), and yellow **3** (6.6 mg, 24%).

Addition of CO to 2. Compound **2** (14.6 mg, 0.0115 mmol) was dissolved in 20 mL of methylene chloride and heated to reflux under a CO atmosphere for 1.5 h. The solvent was then removed in vacuo, and the residue was extracted in methylene chloride and separated by TLC by using 4:1 hexane/methylene chloride (v/v) solvent mixture to give the following products in order of elution: colorless **1** (2.8 mg, 21%), a yellow band of the known compound $PtRe_2(CO)_9(PBu^t_3)(\mu\text{-}H)_2$[8] (1.7 mg, 11%), unreacted orange **2** (3.1 mg, 16%), and brown **3** (1.6 mg, 8%).

Synthesis of $Re_2Pt(PBu^t_3)(Ph)(CO)_8(SbPh_3)(\mu_3\text{-}SbPh)(\mu\text{-}H)$, 5. $SbPh_3$ (15.2 mg, 0.0431 mmol) was added to a solution of **2** (48.3 mg, 0.0380 mmol) in 40 mL of freshly distilled hexane. The reaction was heated to reflux for 2 h. The solvent was then removed in vacuo, and the residue was extracted in methylene chloride and separated by TLC by using 3:1 hexane/methylene chloride (v/v) solvent mixture to give products in order of elution: **1** (4.5 mg, 14%), unreacted **2** (16.7 mg, 35%), and yellow **5** (5.6 mg, 9%). Spectral data for **5.** IR (ν_{CO} in hexane): 2090(w), 2058(w), 2054(w), 2007(vs), 2002(s), 1982(m), 1954(vs), 1921(m), 1907(w), 1896(w) cm^{-1}. ^1H NMR [CD_2Cl_2] $\delta = 7.82-6.78$ (m, Ph, 25 h), 1.53 (d, Bu^t, $^3J_{P-H} = 13.2$ Hz, 27 h), −7.85 (d, hydride, 1H, $^1J_{Pt-H} = 548.8$ Hz, $^2J_{P-H} = 13.6$ Hz), ^{31}P NMR [CD_2Cl_2] $\delta = 82.7$ (s, P, $^1J_{195Pt-H} = 2712.9$ Hz). Mass Spec. TOF/ES: 1663 ($M + K^+$), 1647 ($M + Na^+$), 1588 (M − Ph + NCMe), 1547 (M − Ph).

Addition of CO to 4. Compound **4** (11.2 mg, 0.00625 mmol) was dissolved in 5 mL of methylene chloride. The solution was purged with CO at 25 °C for 20 min. The solvent was then removed in vacuo. The residue was extracted in methylene chloride and separated by TLC by using 3:1 hexane/methylene chloride (v/v) solvent mixture to yield two products, in order of elution: a light yellow band of trans-$[Re(CO)_4Pt(H)(CO)(PBu^t_3)(\mu_3\text{-}SbPh)]_2$, trans-**6** (2.8 mg, 24%), and a light brown band of cis-$[Re(CO)_4Pt(H)(CO)(PBu^t_3)(\mu_3\text{-}SbPh)]_2$, cis-**6** (3.3 mg, 29%). Spectral data for cis-**6:** IR(ν_{CO} cm^{-1} in hexane): 2045(m), 2025(m), 1976(vs), 1964(m), 1932(s) cm^{-1}. ^1H NMR [CD_2Cl_2] $\delta = 7.63-7.11$ (m, Ph, 10H), 1.35 (d, Bu^t, 54H, $^2J_{P-H} = 13$ Hz), −3.73 (d, hydride, 2H, $^1J_{195Pt-H} = 786$ Hz, $^2J_{P-H} = 18$ Hz); ^{31}P NMR [CD_2Cl_2] $\delta = 88.8$ (s, P, $^1J_{195Pt-H} = 2366$ Hz). Mass spectrum: EI/MS *m/z* 1846, 1791(−2CO). The isotope distribution pattern is consistent with the presence of two rhenium, two antimony, and two platinum atoms. Spectral data for trans-**6.** IR(ν_{CO} cm^{-1} in hexane): 2066(vw), 2048(m), 2027(m), 1981(vs), 1970(s), 1963(m), 1950(w), 1932(vs) cm^{-1}. ^1H NMR [CD_2Cl_2] $\delta = 7.68-7.18$ (m, Ph, 10H), 1.52 (d, Bu^t, 54H, $^2J_{P-H} = 13$ Hz), −3.62 (d, hydride, 2H, $^1J_{195Pt-H} = 788$ Hz, $^2J_{P-H} = 20$ Hz); ^{31}P NMR [CD_2Cl_2] $\delta = 88.4$ (s, P, $^1J_{195Pt-H} = 2355$ Hz, $^5J_{P-H} = 16$ Hz). Mass Spec. TOF/ES/MS 1885($M + K^+$), 1864($M + NH_4^+$), 1846(M^+). The isotope pattern is consistent with the presence of two rhenium, two antimony, and two platinum atoms.

Crystallographic Analyses. Single crystals of orange **2**, brown cis-**6**, and colorless trans-**6** suitable for X-ray diffraction were obtained by slow evaporation of solvent from solutions in benzene/octane solvent at 5 °C. Single crystals of yellow **3**, purple **4**, and brown **5** suitable for X-ray diffraction were obtained by slow evaporation of solvent from solutions in methylene chloride/hexane solvent at room temperature. Each data crystal was glued onto the end of a thin glass fiber. X-ray intensity data were measured by using a Bruker SMART APEX CCD-based diffractometer by using Mo Kα radiation ($\lambda = 0.71073$ Å). The raw data frames were integrated with the SAINT+ program by using a narrow-frame integration algorithm.[12] Correction for Lorentz and polarization effects were also applied with SAINT+. An empirical absorption correction based on the multiple measurement of equivalent reflections was applied using the program SADABS. All structures were solved by a combination of direct methods and difference Fourier syntheses, and refined by full-matrix least-squares on F^2,

(12) *SAINT+*, Version 6.2a; Bruker Analytical X-ray System, Inc., Madison, WI, 2001.

using the SHELXTL software package.[13] All non-hydrogen atoms were refined with anisotropic thermal parameters. Unless indicated otherwise, the hydrogen atoms were placed in geometrically idealized positions and included as standard riding atoms during the least-squares refinements. Crystal data, data collection parameters, and results of the refinements are listed in Table 1.

Compounds **2, 3** and **4** all crystallized in the monoclinic crystal system. The space group $P2_1/n$ was confirmed for **2** on the basis of the systematic absences observed in the data. The alternative standard setting of the space group $P2_1/n$, $P2_1/c$ was selected for **3** and **4** on the basis of the systematic absences observed in the data for both of these compounds. The hydrido ligands in **2** were located and refined in the structural analyses using isotropic thermal parameters. Both of the hydrido ligands in **3** and **4** were located in difference Fourier maps. The hydrido ligand in **3** and one of them H(1) in **4** were refined by using the constraint M−H equals 1.75 Å. Compound **5** crystallized in the triclinic crystal system. The space group $P\bar{1}$ was assumed and confirmed by the successful solution and refinement of the structure. Both of the hydrido ligands in **5** were located in a difference Fourier map and were refined by using the constraint M−H equals 1.75 Å. Compound **cis-6** crystallized in the monclinic crystal system in the space group $P2_1/c$. The asymmetric crystal unit contains 1 equiv of the complex together with 2 equiv of benzene that cocrystallized from the crystallization solvent. Both of the hydrido ligands in **cis-6** were located in a difference Fourier map and were refined by using the constraint M−H equals 1.75 Å. Compound **trans-6** crystallized in the triclinic crystal system. The space group $P\bar{1}$ was assumed and confirmed by the successful solution and refinement of the structure. With Z = 1, the asymmetric crystal unit contains only one half of the complex, but also contains one independent equivalent of benzene that cocrystallized from the crystallization solvent. The one independent hydrido ligand was located and refined without contraints.

Molecular Orbital Calculations. The electronic structure of **4** with complete ligands was fully optimized by the density functional theory (DFT) method with the nonempirical meta-GGA Tao-Perdew-Staroverov-Scuseria (TPSS) functional[14] in the Gaussian 03 suite of ab initio programs[15] with the 6−31G(d,p) basis set for H, C, O, and P atoms,[16] the ECP60MWB basis set for Re and Pt

Table 1. Crystallographic Data for Compounds **2**, **3**, **4**, **5**, cis-**6**, and trans-**6**

compound	**2**	**3**	**4**	**5**	cis-**6**	trans-**6**
empirical formula	$PtRe_2SbPO_8C_{32}H_{38}$	$PtRe_2SbPO_9C_{33}H_{38}$	$Pt_2Re_2Sb_2P_2O_8C_{44}H_{64}\cdot{}^1/_2C_6H_{14}$	$PtRe_2Sb_2PO_8C_{50}H_{53}\cdot C_6H_{14}$	$Pt_2Re_2Sb_2P_2O_{10}C_{49}H_{73}\cdot 2C_6H_6$	$Pt_2Re_2Sb_2P_2O_{10}C_{49}H_{73}\cdot 2C_6H_6$
formula weight	1270.83	1298.84	1834.07	1666.97	2003.22	2003.22
crystal system	monoclinic	monoclinic	monoclinic	triclinic	monoclinic	triclinic
lattice parameters						
a (Å)	11.1689(2)	11.4574(4)	20.0255(6)	10.2020(5)	17.539(1)	9.327(2)
b (Å)	17.4875(3)	28.2485(10)	13.6683(4)	14.1979(6)	14.4863(8)	12.241(3)
c (Å)	19.2245(4)	12.8878(4)	21.6654(6)	20.8235(9)	26.508(2)	16.612(4)
α (deg)	90	90	90	81.189(1)	90	108.363(4)
β (deg)	98.606(1)	113.341(1)	96.986(1)	86.292(1)	103.280(1)	94.711(4)
γ (deg)	90	90	90	72.244(1)	90	109.011(4)
V (Å^3)	3712.58(12)	3829.8(2)	5886.1(3)	2838.1(2)	6555.2(6)	1665.4(6)
space group	$P2_1/n$, No. 14	$P2_1/c$, No. 14	$P2_1/c$, No. 14	$P\bar{1}$, No. 2	$P2_1/c$, No. 14	$P\bar{1}$, No. 2
Z value	4	4	4	4	4	1
ρ_{calc} (g/cm^3)	2.274	2.253	2.070	1.951	2.030	1.997
μ (Mo Kα) (mm^{-1})	11.063	10.729	9.834	7.720	8.842	8.701
temperature (K)	294(2)	294(2)	294(2)	293(2)	100(2)	294(2)
$2\Theta_{max}$ (deg)	56.62	56.64	56.66	52.74	52.7	56.5
no. obs. ($I > 2\sigma(I)$)	7228	4923	10731	9279	10603	6997
no. parameters	419	437	580	603	637	356
goodness of fit	1.020	1.059	1.035	1.003	1.045	1.037
max. shift in cycle	0.002	0.001	0.001	0.002	0.003	0.002
residuals^a: R1;wR2	0.0318; 0.0751	0.0438; 0.0908	0.0426; 0.0652	0.0302; 0.0681	0.0421; 0.1020	0.0352; 0.0797
absorption corr., max/min	Multiscan 1.000/0.393	Multiscan 1.000/0.343	Multiscan 1.000/0.212	Multiscan 1.000/0.829	Multiscan 1.000/0.533	Multiscan 1.000/0.520
largest peak in final diff. map (e$^-$/Å^3)	1.739	2.203	3.206	2.010	2.559	1.854

^{a} *$R = \sum_{hkl}(||F_{obs}| - |F_{calc}||)/\sum_{hkl}|F_{obs}|$; $R_w = [\sum_{hkl}w(|F_{obs}| - |F_{calc}|)^2/\sum_{hkl}wF_{obs}{}^2]^{1/2}$, $w = 1/\sigma^2(F_{obs})$; GOF = $[\sum_{hkl}w(|F_{obs}| - |F_{calc}|)^2/(n_{data} - n_{vari})]^{1/2}$.

(13) Sheldrick, G. M. *SHELXTL*, Version 6.1; Bruker Analytical X-ray Systems, Inc., Madison, WI, 1997.

(14) Tao, J. M.; Perdew, J. P.; Staroverov, V. N.; Scuseria, G. E. *Phys. Rev. Lett.* **2003**, *91*, 146401-1–146401-4.

(15) Frisch, M. J.; Trucks, G. W.; Schlegel, H. B.; Scuseria, G. E.; Robb, M. A.; Cheeseman, J. R.; Montgomery, J. A., Jr.; Vreven, T.; Kudin, K. N.; Burant, J. C.; Millam, J. M.; Iyengar, S. S.; Tomasi, J.; Barone, V.; Mennucci, B.; Cossi, M.; Scalmani, G.; Rega, N.; Petersson, G. A.; Nakatsuji, H.; Hada, M.; Ehara, M.; Toyota, K.; Fukuda, R.; Hasegawa, J.; Ishida, M.; Nakajima, T.; Honda, Y.; Kitao, O.; Nakai, H.; Klene, M.; Li, X.; Knox, J. E.; Hratchian, H. P.; Cross, J. B.; Adamo, C.; Jaramillo, J.; Gomperts, R.; Stratmann, R. E.; Yazyev, O.; Austin, A. J.; Cammi, R.; Pomelli, C.; Ochterski, J. W.; Ayala, P. Y.; Morokuma, K.; Voth, G. A.; Salvador, P.; Dannenberg, J. J.; Zakrzewski, V. G.; Dapprich, S.; Daniels, A. D.; Strain, M. C.; Farkas, O.; Malick, D. K.; Rabuck, A. D.; Raghavachari, K.; Foresman, J. B.; Ortiz, J. V.; Cui, Q.; Baboul, A. G.; Clifford, S.; Cioslowski, J.; Stefanov, B. B.; Liu, G.; Liashenko, A.; Piskorz, P.; Komaromi, I.; Martin, R. L.; Fox, D. J.; Keith, T.; Al-Laham, M. A.; Peng, C. Y.; Nanayakkara, A.; Challacombe, M.; Gill, P. M. W.; Johnson, B.; Chen, W.; Wong, M. W.; Gonzalez, C.; Pople, J. A. *Gaussian 03, revision C.02, suite of programs for ab initio calculation*; Gaussian, Inc.: Wallingford CT, 2004.

(16) (a) Hehre, W. J.; Ditchfield, R.; Pople, J. A. *J. Chem. Phys.* **1972**, *56*, 2257. (b) Francl, M. M.; Petro, W. J.; Hehre, W. J.; Binkley, J. S.; Gordon, M. S.; DeFrees, D. J.; Pople, J. A. *J. Chem. Phys.* **1982**, *77*, 3654–3665.

atoms,[17] and the ECP28MDF_VTZ basis set for the Sb atom.[18] Then, to simplify the bonding analysis of this cluster, the fragment analysis of the ADF program[19] was used for a single point calculation with the Perdew-Burke-Ernzerhof (PBE) functional[20] in Slater-type triple-ζ all-electron one polarization function (TZP) basis set with the zeroth-order regular approximation (ZORA) for relativistic effect on a smaller C_2 symmetry model, where H replaced the phenyl rings and *t*-butyl groups.

Fenske−Hall calculations were performed utilizing a graphical user interface developed to build inputs and view outputs from stand-alone Fenske−Hall and MOPLOT2 binary executables.[21,22] Contracted double-ζ basis sets were used for the Re 5d, Pt 5d, Sb 5p, P 3p, and C and O 2p atomic orbitals. The Fenske−Hall scheme is a nonempirical approximate method that is capable of calculating molecular orbitals for very large transition metal systems. For these calculations, the input structures were obtained from the positional parameters from the crystal structure analyses. The structures are not optimized by these calculations. The *t*-butyl groups on the phosphine ligands and the phenyl groups on the $SbPh_2$ ligand were replaced with hydrogen atoms, for example, PH_3, SbH_2, and SbH, for these calculations.

Results and Discussion

The major product obtained from the reaction of **1** with $Pt(PBu^t_3)_2$ is the compound $Re_2[Pt(PBu^t_3)](\mu\text{-}SbPh_2)(CO)_8(\mu\text{-}H)$, **2** (39% yield). Two minor products, $Re_2[Pt(CO)(PBu^t_3)]Ph(CO)_8(\mu_3\text{-}SbPh)(\mu\text{-}H)$, **3** (4% yield) and $Re_2[Pt(PBu^t_3)]_2(CO)_8(\mu_4\text{-}Sb_2Ph_2)(\mu\text{-}H)_2$, **4** (1% yield) were also obtained. Compound **3** was subsequently obtained from **2** by further reaction with $Pt(PBu^t_3)_2$, see below. Compound **2** was characterized by IR and ^{1}H NMR spectroscopy and by elemental and single crystal X-ray diffraction analyses.

An Oak Ridge Thermal Ellipsoid Plot (ORTEP) diagram of the molecular structure of **2** is shown in Figure 1. The molecule contains a triangular cluster of three metal atoms, two of rhenium and one of platinum, with a bridging $SbPh_2$ ligand across one of the rhenium−platinum bonds and a bridging hydrido ligand across the other rhenium−platinum bond. Compound **2** is similar to the compound $PtRe_2(CO)_9(PBu^t_3)(\mu\text{-}H)_2$, **7**, which contains an additional CO ligand and a hydrido ligand instead of the $SbPh_2$ ligand.[8] A comparison of the structures of **2** and **7** shows the following: the Re−Re bond in **2**, Re(1)−Re(2) = 3.0866(3) Å, is considerably shorter than the hydride bridged Re−Re bond in **7**, Re(1)−Re(2) = 3.1726(4) Å; the hydride-bridged Re−Pt bond in **2**, Pt(1)−Re(1) = 2.7839(3) Å, is considerably shorter than the hydride-bridged Re−Pt bond in **7**, Pt−Re = 2.9667(4) Å. The reason for this is not clear, but this may be related to the remaining ligand structure, particularly, the presence of the additional terminal CO ligand on the platinum atom in **7** versus the bridging $SbPh_2$ ligand in **2**. Interestingly, the $SbPh_2$ bridged Pt−Re bond in **2**, Pt(1)−Re(2) = 2.9265(3) Å, is considerably longer than the unbridged Pt−Re bond in **7**, 2.8133(4) Å. The Re−Sb bond distance in **2**, Re(2)−Sb(1) = 2.6863(5) Å, is very similar to the Re−Sb distances found in **1**, Re−Sb = 2.6934(7)−2.6983(7) Å.[11] The Pt−Sb distance is considerably shorter, 2.5160(4) Å, than the Re−Sb bond distance. The hydrido ligand was located and refined structurally, Pt(1)−H(1) = 1.76(8), Re(1)−H(1) = 1.90(8), and it exhibits the expected high-field resonance shift, δ = −8.00 with appropriate couplings to platinum and phosphorus, $^1J_{Pt-H}$ = 990 Hz, $^2J_{P-H}$ = 10 Hz in the ^{1}H NMR spectrum. The phosphine ligand displays the expected ^{31}P NMR shift, δ = 124.21 with suitable coupling to ^{195}Pt, $^1J_{Pt-P}$ = 3735 Hz. When heated to reflux in an octane solution (125 °C), compound **2** was converted back to **1** in 52% yield together with the formation of a small amount of **3** (10% yield).

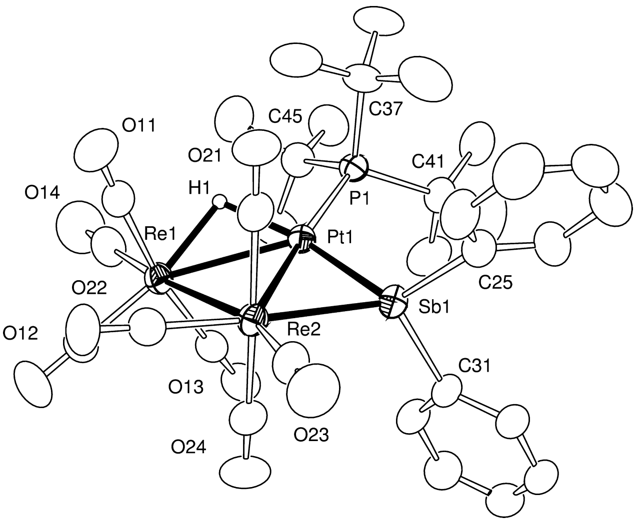

Figure 1. ORTEP diagram of the molecular structure of **2** showing 40% probability thermal ellipsoids. The hydrogen atoms on the ligands are omitted for clarity. Selected bond distances (Å) and angles (deg) are as follows: Pt(1)−Re(1) = 2.7839(3), Pt(1)−Re(2) = 2.9265(3), Re(1)−Re(2) = 3.0866(3), Pt(1)−Sb(1) = 2.5160(4), Re(2)−Sb(1) = 2.6863(5), Pt(1)−P(1) = 2.3060(15), Pt(1)−H(1) = 1.76(8), Re(1)−H(1) = 1.90(8).

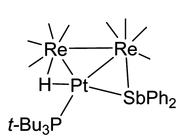

2

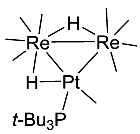

7

An ORTEP diagram of the molecular structure of **3** is shown in Figure 2. The molecule contains an open cluster of three metal atoms, two of rhenium and one of platinum, with a triply bridging SbPh ligand. The platinum atom is bonded to one of the rhenium atoms, Pt(1)−Re(1) = 3.0082(5) Å. This bond is only slightly longer, 0.042 Å, than the hydride bridged Pt−Re bond distance in **7**, and this bond contains both a bridging

(17) (a) Andrae, D.; Haeussermann, U.; Dolg, M.; Stoll, H.; Preuss, H. *Theor. Chim. Acta* **1990**, *77*, 123–141. (b) Martin, J. M. L.; Sundermann, A. *J. Chem. Phys.* **2001**, *114*, 3408–3420.
(18) Peterson, K. A. *J. Chem. Phys.* **2003**, *119*, 11099–11112.
(19) Baerends, E. J. et al. *ADF, revision 2007.01, SCM*; Theoretical Chemistry, Vrije Universiteit: Amsterdam, The Netherlands, 2007; http://www.scm.com.
(20) (a) Perdew, J. P.; Burke, K.; Ernzerhof, M. *Phys. Rev. Lett.* **1996**, *77*, 3865–3868. (b) Perdew, J. P.; Burke, K.; Ernzerhof, M. *Phys. Rev. Lett.* **1997**, *78*, 1396–1396.
(21) *JIMP2, a free program for visualizing and manipulating molecules*, version 0.091Hall, M. B.; Fenske, R. F. *Inorg. Chem.* **1972**, *11*, 768–779. Manson, J.; Webster, C. E.; Hall, M. B. Texas A&M University: College Station, TX, 2006; http://www.chem.tamu.edu/jimp2/index.html.
(22) *MOPLOT2 for orbital and density plots from linear combinations of Slater or Gaussian type orbitals*, version 2.0; Lichtenberger, D. L.; Department of Chemistry, University of Arizona: Tucson, AZ, 1993.

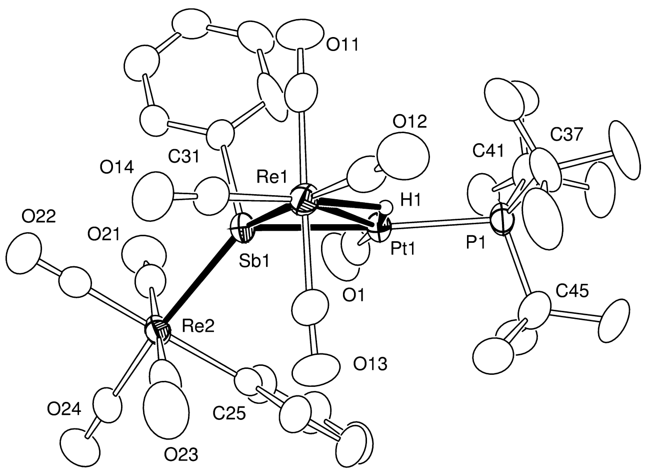

Figure 2. ORTEP diagram of the molecular structure of **3** showing 30% probability thermal ellipsoids. The hydrogen atoms on the ligands are omitted for clarity. Selected interatomic bond distances (Å) and angles (deg) are as follows: Pt(1)−Re(1) = 3.0082(5), Re(1)−Sb(1) = 2.6885(7), Re(2)−Sb(1) = 2.7404(6), Pt(1)−Sb(1) = 2.6499(6), Re(2)−C(25) = 2.228(9), Pt(1)−P(1) = 2.399(2), Pt(1)−C(1) = 1.865(11), Pt(1)−H(1) = 1.75(2), Re(1)−H(1) = 1.75(2); Pt(1)−Sb(1)−Re(1) = 68.592(17), Pt(1)−Sb(1)−Re(2) = 126.71(2), Re(1)−Sb(1)−Re(2) = 130.33(2).

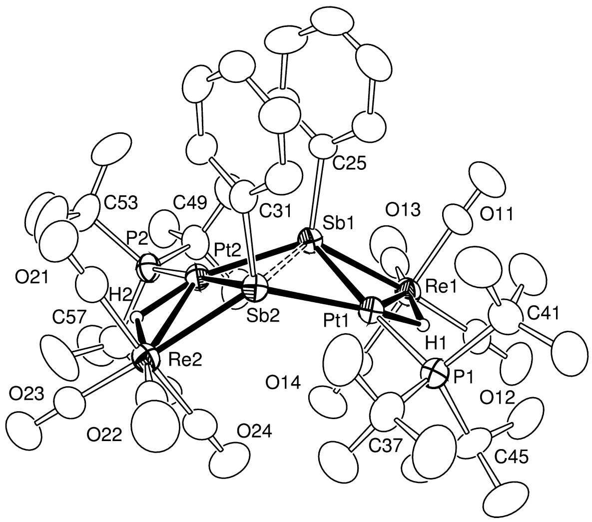

Figure 3. ORTEP diagram of the molecular structure of **4** showing 30% probability thermal ellipsoids. The hydrogen atoms on the ligands are omitted for clarity. Selected interatomic bond distances (in Å) are as follows: Pt(1)−Re(1) = 3.0116(5), Pt(2)−Re(2) = 2.9865(5), Pt(1)−Sb(1) = 2.6474(6), Pt(1)−Sb(2) = 2.6003(6), Pt(2)−Sb(1) = 2.5927(6), Pt(2)−Sb(2) = 2.6549(6), Re(1)−Sb(1) = 2.6945(6), Re(2)−Sb(2) = 2.6905(6), Sb(1)−Sb(2) = 2.9834(7), Re(1)−H(1) = 1.75(1). Re(2)−H(2) = 1.91(6), Pt(1)−H(1) = 1.75(1), Pt(2)−H(2) = 1.65(7), Pt(1)−P(1) = 2.367(2), Pt(2)−P(2) = 2.370(2).

hydrido ligand and a terminal CO ligand on the platinum atoms, as in **7**. Atom Re(2) is linked to the cluster solely via the bridging SbPh ligand. The Re−Sb distance, Re(2)−Sb(1) = 2.7404(6) Å, is slightly longer than the Re−Sb distance in **2** and the other Re−Sb distance in **3**, Re(1)−Sb(1) = 2.6885(7) Å. There is a σ-phenyl ligand on Re(2) that was evidently cleaved from the $SbPh_2$ ligand in **2**, Re(2)−C(25) = 2.228(9) Å. The hydrido ligand in **3** exhibits the expected high field resonance shift, $\delta = -8.02$, with couplings to ^{31}P and ^{195}Pt, $^{2}J_{P-H} = 13$ Hz, $^{1}J_{Pt-H} = 552$ Hz. Compound **3** contains one more CO ligand than **2**, and **3** was also obtained from **2** in a low yield (8%) from the reaction of **2** when CO was added to solutions of **2**.

The structure of compound **4** is unusual. An ORTEP diagram of its molecular structure is shown in Figure 3. The molecule contains four metal atoms, two of rhenium and two of platinum, with two bridging SbPh groups. The molecule can be viewed as a dimer of the fragment $Re[Pt(PBu^t_3)](CO)_4(SbPh)(\mu\text{-}H)$ that could be formed by the elimination of the $Re(CO)_4Ph$ group and a CO ligand from **3**, but efforts to obtain **4** directly from **3** were unsuccessful. The two halves of the molecule are held together by Pt−Sb bonds and a significant direct interaction between the Sb atoms. Each rhenium atom is bonded to one platinum atom, and each Re−Pt bond contains one bridging hydrido ligand. The Re−Pt distances, Pt(1)−Re(1) = 3.0116(5) Å, Pt(2)−Re(2) = 2.9865(5) Å, are similar to the hydride bridged Re−Pt bond distance observed in **7**. The hydrido ligands were located and refined in the structural analysis, Re(1)−H(1) = 1.75(1) Å, Re(2)−H(2) = 1.91(6) Å, Pt(1)−H(1) = 1.75(1) Å, and Pt(2)−H(2) = 1.65(7) Å. The two hydrido ligands are chemically equivalent and exhibit a single sharp high-field resonance in the ^{1}H NMR spectrum at $\delta = -8.27$ with appropriate couplings to ^{195}Pt and ^{31}P, $^{1}J_{Pt-H} = 708$ Hz, $^{2}J_{P-H} = 10$ Hz. The Re−Sb bond distances Re(1)−Sb(1) = 2.6945(6) Å and Re(2)−Sb(2) = 2.6905(6) Å are very similar to those in **1** and **2**. The Pt−Sb distances, Pt(1)−Sb(1) = 2.6474(6) Å, Pt(1)−Sb(2) = 2.6003(6) Å, Pt(2)−Sb(1) = 2.5927(6) Å, and Pt(2)−Sb(2) = 2.6549(6) Å, are slightly longer than that in **2** but are similar to that in **3**. The Sb−Sb distance, 2.9834(7) Å, is sufficiently short to conclude that there is significant bonding directly between these atoms. The Sb−Sb distance in **4** lies in between the two Sb−Sb distances, 2.926(2) Å and 3.155(1) Å, observed for Sb−Sb bonds in the two bridging tetraphenyldistibine ligands found in the compound $Rh_2(COD)_2(Sb_2Ph_4)_2$.[23] It is difficult to draw a rational model for the bonding in **4** containing Sb−Sb bond based on a simple arrangement of two-center two electron bonds. The two structures **4a** and **4b** shown below do not explain the apparent Sb−Sb interaction and its diamagnetic properties. In the structure **4a** the rhenium atoms have 18 electrons and the platinum atoms have 16 electrons but there is no Sb−Sb bond. Although there is a Sb−Sb bond in the structure **4b** and the rhenium atoms would have 18 electron configurations, the platinum atoms would have only 15 electron configurations which should result in paramagnetism that was not indicated because of the sharp ^{1}H NMR resonances. Also, structure **4b** would have no bond between the antimony atom and the second platinum atom.

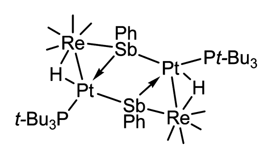

4a

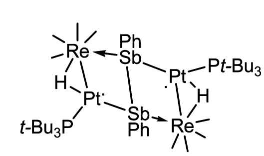

4b

(23) Sharma, P.; Rosas, N.; Hernandez, S.; Cabrera, A. *J. Chem. Soc.,Chem. Commun.* **1995**, 1325–1326.

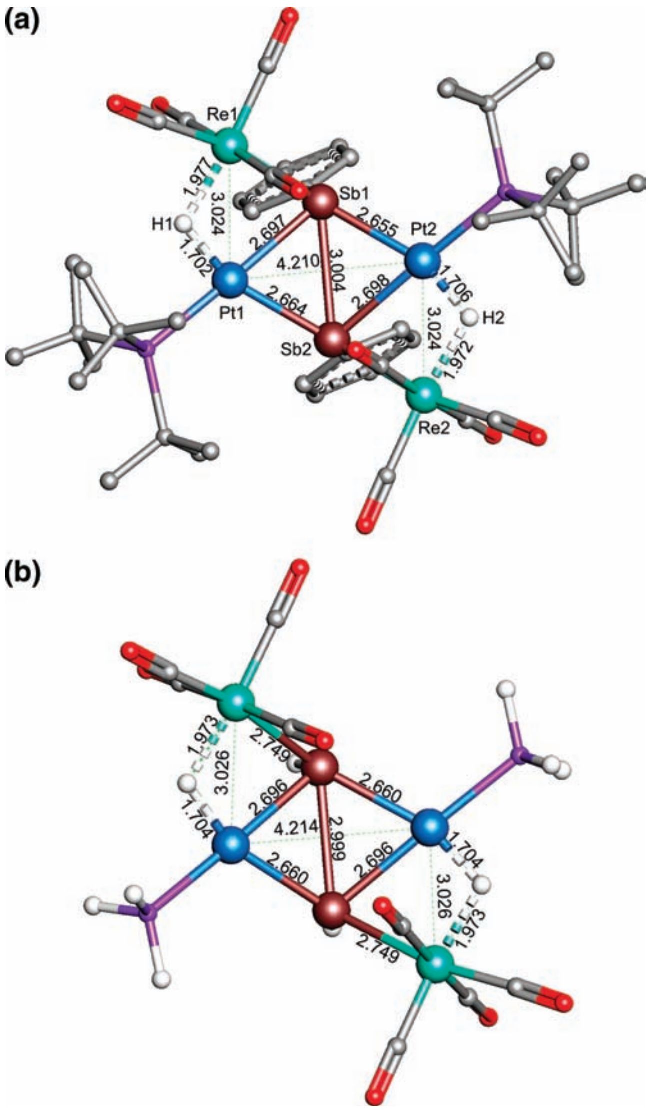

Figure 4. JIMP2 representation of the optimized structure of **4** and its simplified model. Bond lengths shown in this figure are angstrom. (a) With full ligands. The hydrogen atoms on the phenyl rings and *t*-butyl groups were removed for clarity. (b) Simplified model (H replaced the phenyl rings and *t*-butyl groups) with C_2 symmetry.

Accordingly, the electronic structure of **4** was investigated computationally by using DFT. The fully optimized structure of **4** and a few key computed geometric parameters are shown in Figure 4. The optimized Sb−Sb distance of 3.00 Å is only slightly longer than the distance 2.9834(7) Å observed in the crystal structure analysis. As shown in Scheme 1, our analysis of the cluster bonding was based on breaking the cluster into two identical symmetric fragments (A and B) by cutting the molecule in two through a plane that passes between the Sb and the Pt atoms, nearly perpendicular to the Sb−Re bond. The bonding within each fragment can be represented as a $HRe^{I}(CO)_4$ (d^6, pseudo octahedral fragment) bonded to the $Pt^{II}(PR_3)$ through the HRe by a 3-center, 2-electron bond. The $[SbR']^{2-}$ unit bonds to the Re and Pt through donation of lone pairs to Re and Pt. This resulting fragment has an unused Sb lone pair and an unused empty Pt orbital. These orbitals are the highest occupied molecular orbital (HOMO) and the lowest unoccupied molecular orbital (LUMO), respectively, of the half-molecule fragments and are displayed at the bottom of Scheme 1. On

Scheme 1. Orbital Interaction Diagram of **4**[a]

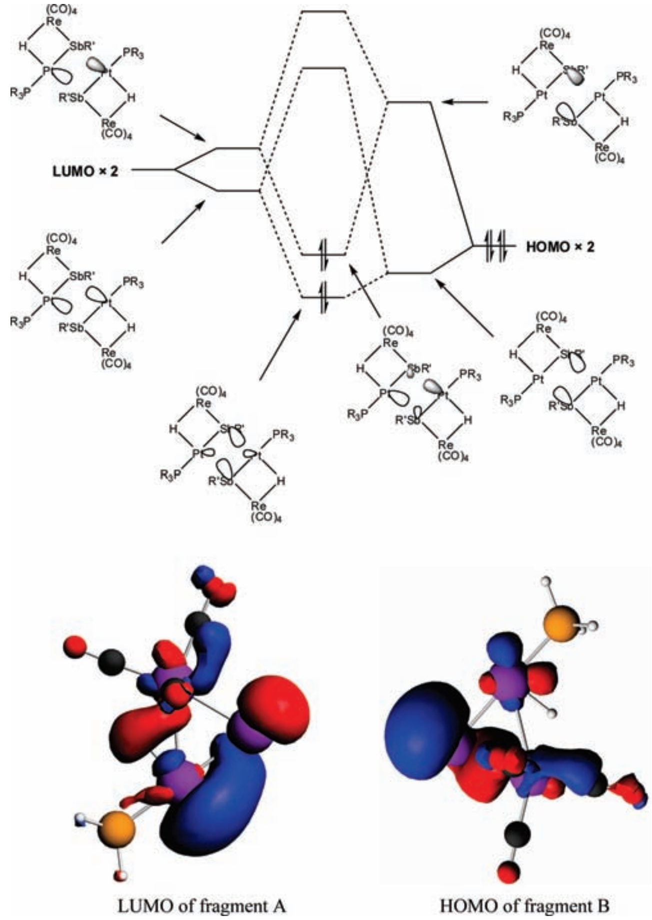

[a] Occupation number: Sb HOMO 2.0 → 1.34; Pt LUMO 0.0 → 0.76.

the basis of the fragment analysis, there is a strong interaction between the two Sb lone pairs resulting in a large splitting between the in-phase and out-of-phase combinations, as shown on the right side of Scheme 1. The interaction between the two Pt orbitals is smaller as shown on the left side of Scheme 1. Finally, there is a small interaction between the in-phase Sb−Sb combination and the in-phase Pt−Pt combination, which produces the lowest lying orbital, and a larger interaction between the more closely spaced out-of-phase combinations, which results in the higher lying occupied orbital as shown in the MO diagram (Scheme 1). These four electrons constitute the main interactions holding the two fragments together. There is a significant net Sb−Sb bonding as the in-phase Sb−Sb combination makes a larger overall contribution in the two occupied molecular orbitals, while both occupied orbitals contribute to Sb−Pt bonding. The final population analysis in the fragment basis set supports these conclusions as these are the only fractionally occupied orbitals. The previously unused empty Pt orbitals, shown as the LUMO on fragment A (Scheme 1), gain ∼0.7 electrons each in this interaction, while the Sb lone pairs, shown as the HOMO of fragment B (Scheme 1), lose ∼0.7 electrons each. The MOs of the whole cluster do not have orbitals corresponding exactly to these two fragments' interactions as shown in Scheme 1 because those interactions become strongly mixed with numerous other MOs when the fragments are combined. However, the fragment population

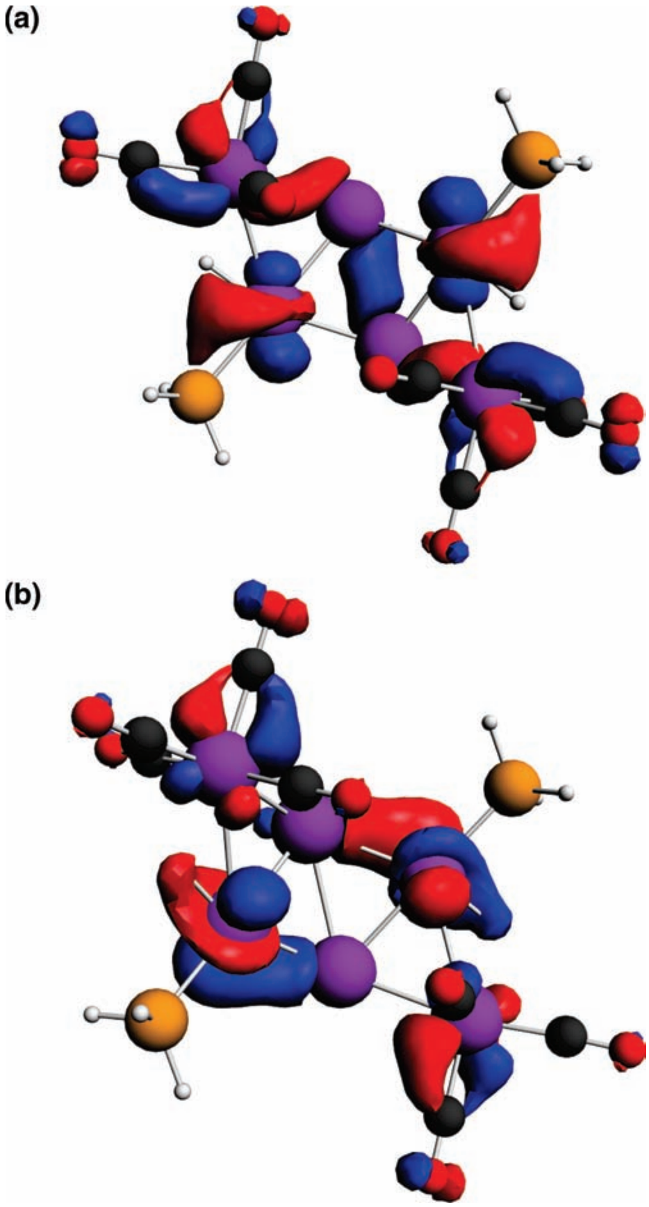

Figure 5. (a) Contour diagram of the HOMO-1 orbital of the modeled structure of **4** calculated by ADF showing significant Sb−Sb bonding. (b) Contour diagram of the HOMO-4 orbital of the modeled structure of **4** calculated by ADF showing significant Sb−Pt bonding.

analysis described above suggests that this mixing does not change the net bonding description as no other occupied fragment orbitals lose more than ∼0.03 electrons and no other unoccupied fragment orbitals gain more than ∼0.03 electrons. A significant fraction of the net Sb−Sb and Sb−Pt bonding can be seen in the HOMO-1 and HOMO-4, respectively, as shown in Figure 5. To verify the validity of the fragment analysis using this simplified model, the molecular orbitals of **4** with the complete ligands optimized by Gaussian 03 were calculated. Two similar orbitals, HOMO-1 and HOMO-2, with significant fractions of the net Sb−Sb and Sb−Pt bonding, respectively, were found. These are shown in Figure 6. In summary, by creating two delocalized MOs that are filled by four electrons, the molecule is able to form a Sb−Sb bond that is accompanied by sufficient Pt−Sb bonding to produce the observed pairing of all electrons in the compound.

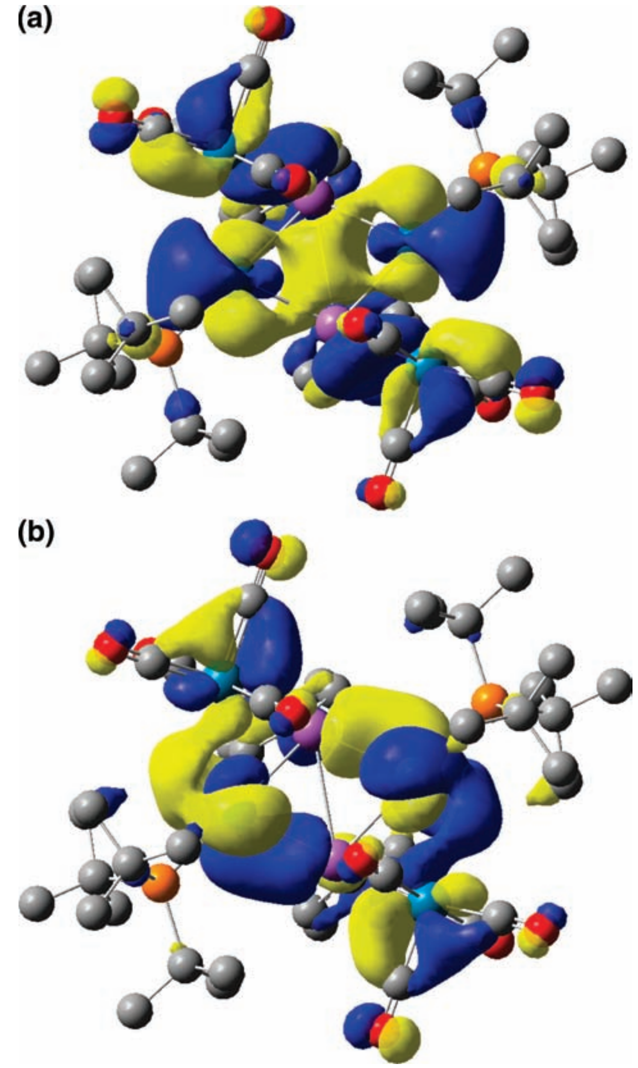

Figure 6. (a) Contour diagram of the HOMO-1 orbital of **4** optimized by Gaussian 03 showing significant Sb−Sb bonding. (b) Contour diagram of HOMO-2 orbital of **4** optimized by Gaussian 03 showing significant Sb−Pt bonding.

The reaction of **2** with $SbPh_3$ was also investigated. This reaction proceeds similarly to that of the addition of CO to **2**. This reaction yields the open cluster **5** which is structurally similar to **3** except that it contains a $SbPh_3$ ligand instead of CO on the pendant rhenium group. The structure of **5** was determined crystallographically, and an ORTEP diagram of its molecular structure is shown in Figure 7. Compound **5** contains two rhenium atoms and one platinum atom. The platinum atom is bonded to one of the rhenium atoms, Pt(1)−Re(1) = 3.0033(4) Å, and the three metal atoms are held together by a triply bridging SbPh ligand, Re(1)−Sb(1) = 2.7001(5) Å, Re(2)−Sb(1) = 2.7477(5) Å, and Pt(1)−Sb(1) = 2.6683(5) Å. Atom Re(2) contains a σ-phenyl group, Re(2)−C(30) = 2.219(7) Å, a $SbPh_3$ ligand, Re(2)−Sb(2) = 2.7074(5) Å, and three linear terminal carbonyl ligands. The phenyl group and the $SbPh_3$ ligand lie cis to the bridging antimony atom Sb(1). There is one hydrido ligand that bridges the Pt(1)−Re(1) bond. The ligand was located crystallographically but could be refined only with the restraint M−H = 1.75 Å. The ligand exhibits the expected

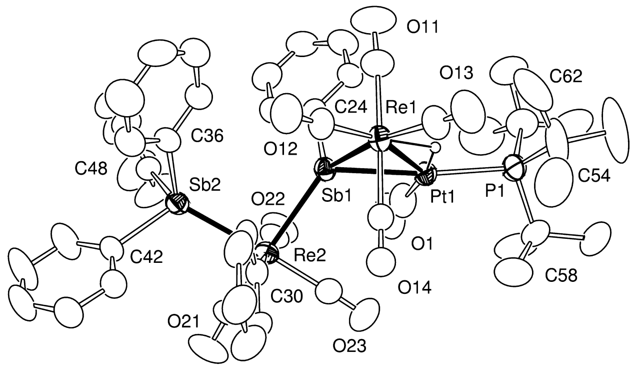

Figure 7. ORTEP diagram of the molecular structure of **5** showing 30% probability thermal ellipsoids. The hydrogen atoms on the ligands are omitted for clarity. Selected interatomic bond distances (Å) and angles (deg) are as follows: Pt(1)−Re(1) = 3.0033(4), Re(1)−Sb(1) = 2.7001(5), Re(2)−Sb(1) = 2.7477(5), Pt(1)−Sb(1) = 2.6683(5), Re(2)−C(30) = 2.219(7), Pt(1)−P(1) = 2.390(2), Pt(1)−C(1) = 1.841(9), Pt(1)−H(1) = 1.75(2), Re(1)−H(1) = 1.75(2); Pt(1)−Sb(1)−Re(1) = 68.03(1), Pt(1)−Sb(1)−Re(2) = 119.69(2), Re(1)−Sb(1)−Re(2) = 131.40(2).

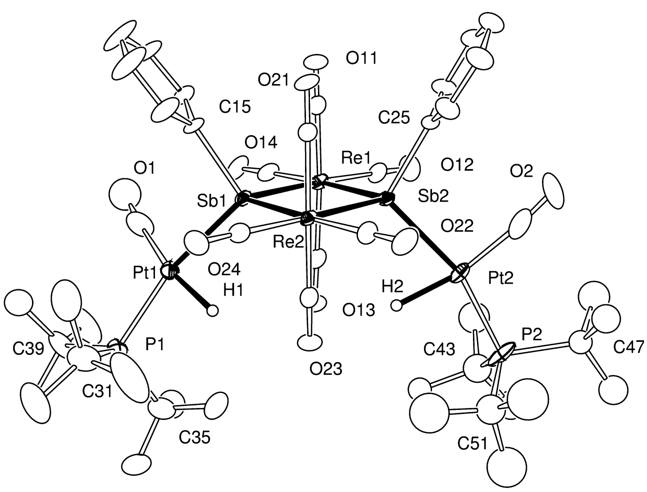

Figure 8. ORTEP diagram of the molecular structure of cis-**6** showing 30% probability thermal ellipsoids. The hydrogen atoms on the ligands are omitted for clarity. Selected interatomic bond distances (Å) and angles (deg) are as follows: Pt(1)−Sb(1) = 2.6062(6), Pt(2)−Sb(2) = 2.5957(6), Re(1)−Sb(1) = 2.7660(6), Re(1)−Sb(2) = 2.7794(7), Re(2)−Sb(1) = 2.7685(7), Re(2)−Sb(2) = 2.7804(7), Pt(1)−P(1) = 2.334(2), Pt(2)−P(2) = 2.351(3), Pt(1)−C(1) = 1.866(10), Pt(2)−C(2) = 1.917(12), Re(1)···Re(2) = 4.319(1), Sb(1)···Sb(2) = 3.481(1); P(1)−Pt(1)−Sb(1) = 160.64(7), P(2)−Pt(2)−Sb(2) = 162.43(9), Re(1)−Sb(1)−Re(2) = 102.59(2), Re(1)−Sb(2)−Re(2) = 101.94(2).

high field shift in the ^{1}H NMR spectrum, $\delta = -7.85$ with the expected couplings to ^{195}Pt, 548.8 Hz and ^{31}P, 13.6 Hz.

Two isomers of $[Re(CO)_4Pt(H)(CO)(PBu^t_3)(\mu_3\text{-}SbPh)]_2$, cis-**6** (29% yield) and trans-**6** (24% yield), were obtained from the reaction of **4** with CO at 1 atm/25 °C in a CH_2Cl_2 solution. Compounds cis-**6** and trans-**6** were formed by the addition of 2 equiv of CO to **4**, one to each platinum atom. Both compounds were characterized by a combination of IR, ^{1}H NMR, mass spectra, and single-crystal X-ray diffraction analyses.

An ORTEP diagram of the molecular structure of cis-**6** is shown in Figure 8. Compound cis-**6** contains two $Re(CO)_4$ groups that are held together by two bridging SbPh ligands. The rhenium−rhenium distance, Re(1)···Re(2) = 4.319(1) Å is clearly nonbonding. The Re−Sb bond distances Re(1)−Sb(1) = 2.7660(6), Re(1)−Sb(2) = 2.7794(7), Re(2)−Sb(1) = 2.7685(7) Re(2)−Sb(2) = 2.7804(7)Å are slightly longer than those in **1**, **2**, and **4** but are similar to the long Re−Sb bond in **3** and **5**. The Sb−Sb distance in cis-**6**, 3.481(1) Å, is 0.5 Å longer than that in **4** and is now outside the range of the normal bonding distances. A square planar $Pt(H)(CO)(PBu^t_3)$ group is coordinated to each bridging SbPh ligand. Both platinum groups lie on the same side of the Re_2Sb_2 plane, hence the description as a cis-structure. The two independent Pt−Sb distances, Pt(1)−Sb(1) = 2.6062(6) Å and Pt(2)−Sb(2) = 2.5957(6) Å, are similar to those in **1**−**4**. The bulky PBu^t_3 ligand lies trans to the antimony atom on each platinum atom, P(1)−Pt(1)−Sb(1) = 160.64(7)°, P(2)−Pt(2)−Sb(2) = 162.43(9)°, Pt(1)−P(1) = 2.334(2) Å and Pt(2)−P(2) = 2.351(3) Å. A carbonyl ligand and one terminally coordinated hydrido ligand lie cis to the antimony atom on each platinum atom. The two hydrido ligands are equivalent and exhibit a single high-field resonance in the ^{1}H NMR spectrum $\delta = -3.73$ with suitable one bond coupling to ^{195}Pt, $^1J_{Pt-H} = 786$ Hz and two bond coupling to ^{31}P, $^2J_{P-H} = 18$ Hz.

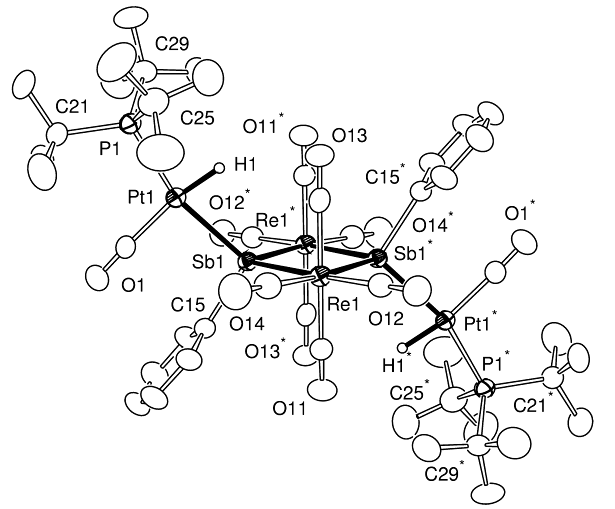

Figure 9. ORTEP diagram of the molecular structure of trans-**6** showing 30% probability thermal ellipsoids. The hydrogen atoms on the ligands are omitted for clarity. Selected interatomic bond distances (Å) and angles (deg) are as follows: Pt(1)−Sb(1) = 2.6113(5), Re(1)−Sb(1) = 2.7858(6), Re(1*)−Sb(1) = 2.7900(6), Pt(1)−C(1) = 1.890(7), Pt(1)−H(1) = 1.42(7), Pt(1)−P(1) = 2.3531(14), Re(1)···Re(2) = 4.339(1), Sb(1)···Sb(2) = 3.501(1); Re(1)−Sb(1)−Re(1*) = 102.20(2), P(1)−Pt(1)−Sb(1) = 163.13(4).

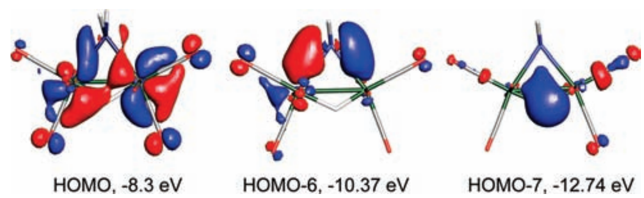

Figure 10. Contour diagrams for some selected Fenske−Hall bonding molecular orbitals of **1** with their calculated energies: (a) HOMO, (b) HOMO-6, (c) HOMO-7, and the (d) HOMO-8.

An ORTEP diagram of the molecular structure of trans-**6** is shown in Figure 9. Compound trans-**6** is structurally similar to cis-**6** in that it contains a central $[PhSbRe(CO)_4]_2$ core that is held together by the two bridging SbPh ligands, and there is a square planar $Pt(H)(CO)(PBu^t_3)$ group coordinated to each bridging SbPh ligand. The most significant difference between the structures of cis-**6** and trans-**6** is that the two $Pt(H)(CO)(PBu^t_3)$ groups lie on the same side of the Re_2Sb_2 plane in cis-**6**

Scheme 2

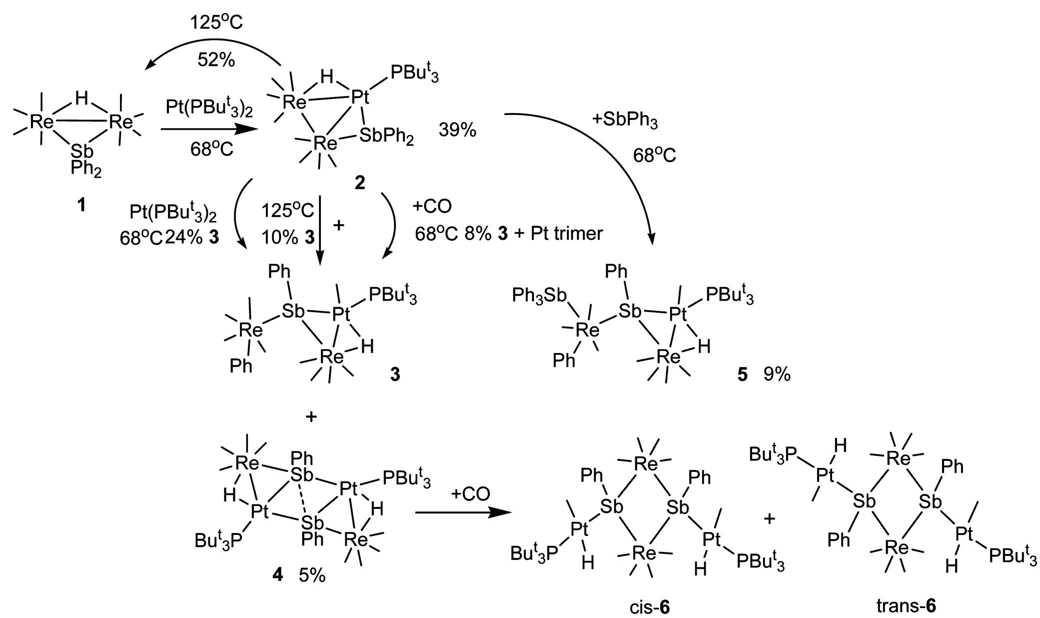

and on opposite sides of the Re_2Sb_2 plane in trans-**6**. In the solid state, trans-**6** is crystallographically centrosymmetrical. The rhenium−rhenium nonbonding distance, Re(1)···Re(1*) = 4.339(1) Å, and the two independent Re−Sb bonding distances, Re(1)−Sb(1) = 2.7858(6) Å, Re(1*)−Sb(1) = 2.7900(6) Å, are virtually the same as those in cis-**6**. The nonbonding Sb···Sb distance in trans-**6** is 3.501(1) Å, only 0.02 Å longer than that in cis-**6**. The square planar $Pt(H)(CO)(PBu^t_3)$ group is coordinated to each bridging SbPh ligand. The one independent Pt−Sb distance is 2.6113(5) Å in length. The one crystallographically independent hydrido ligand was located and refined structurally, Pt(1)−H(1) = 1.42(7) Å. The two hydrido ligands are symmetry equivalent and exhibit a single high-field resonance in the ^1H NMR spectrum, $\delta = -3.62$, with appropriate one bond coupling

Scheme 3

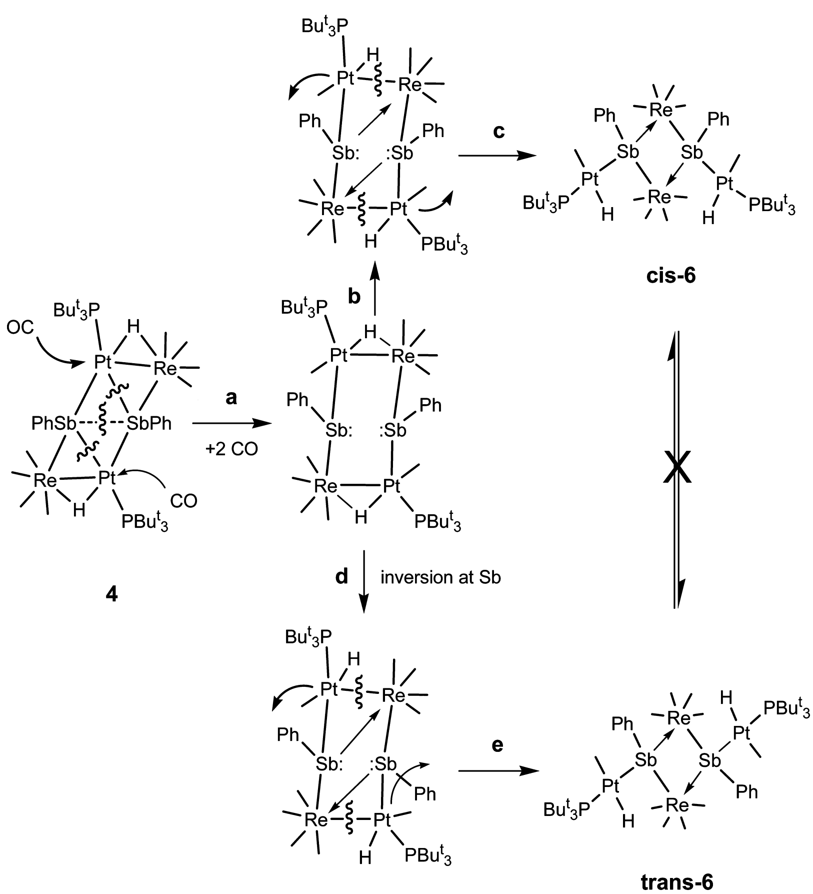

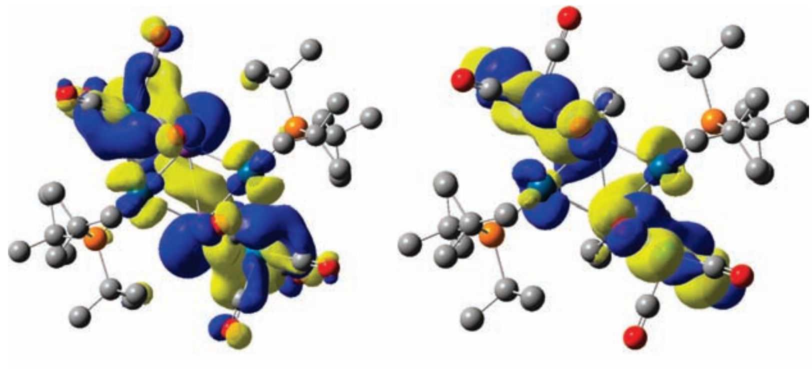

Figure 11. Contour diagrams of the LUMO (left) and LUMO+1 (right) of **4** optimized by Gaussian 03.

to ^{195}Pt, 788 Hz, and two bond coupling to ^{31}P, 20 Hz. As in cis-**6**, the bulky PBu^t_3 ligand lies trans to the antimony atom, P(1)−Pt(1)−Sb(1) = 163.13(4)°, Pt(1)−P(1) = 2.3531(14) Å.

A summary of the reactions described in this paper is shown collectively in Scheme 2.

Compound **2** was formed by the insertion of the platinum atom of a $Pt(PBu^t_3)$ group into one of the Re−Sb bonds of **1**. This step resembles the insertion of the $Pt(PBu^t_3)$ group into one of the hydride bridged Re−Re bonds of $Re_3(CO)_{12}(\mu\text{-}H)_3$, eq 6, but unlike that reaction it was not the hydride-bridged Re−Re bond in **1** where this insertion occurred. To try to obtain an explanation for this, we calculated the molecular orbitals of **1** by the Fenske−Hall method.[21] Contour diagrams of the HOMO of **1** and two other key cluster bonding orbitals, the HOMO-6 and HOMO-7, are shown in Figure 8. The HOMO at $E = -8.3$ eV is dominated by bonding interactions between the rhenium atoms and the bridging $SbPh_2$ ligand and π-bonding to the CO ligands. This could explain the preference for addition of the $Pt(PBu^t_3)$ group at the Re−Sb bonds. The HOMO-6 at −10.37 eV contains substantial Re−Sb overlaps. The orbital that shows the bonding of the hydrido ligand to the rhenium atoms does not appear in the HOMO-7 at −12.74 eV. Because of its low energy, it is less likely that the $Pt(PBu^t_3)$ group will find favorable bonding interactions to HOMO-7 and thus it is less likely that there will be a reaction in the vicinity of the H-bridged Re−Re bond. Reaction 6 is partially reversible. The addition of the $Pt(PBu^t_3)$ to **1** is also partially reversible. When heated to 125 °C, compound **2** was converted back to **1** in 52% yield with a simultaneous formation of a small amount of **3**. The formation of **3** requires the addition of 1 equiv of CO to **2**. Indeed compound **3** can be obtained from **2** by reaction with CO, but the yield is not high, only 8%, and the major product formed from the reaction of **2** with CO is still **1**. The best yield of **3** (24%) was obtained from the reaction of **2** with additional quantities of $Pt(PBu^t_3)_2$. This may be simply because the additional $Pt(PBu^t_3)_2$ inhibits the conversion of **2** back to **1** which simply improves chances for the formation of **3**. The cluster of **2** was also opened by reaction with $SbPh_3$ to give **5** which is simply a $SbPh_3$ derivative of **3**.

A mechanism to explain the formation the compounds cis-**6** and trans-**6** by the addition of CO to **4** is shown in Scheme 3. The addition of CO probably occurs at the 16-electron platinum atoms. The two CO additions may occur sequentially or simultaneously. These additions induce cleavage of one of Pt−Sb bonds to each platinum atom and perhaps the Sb−Sb bond too, step **a**. Examination of the LUMO of **4** shown in Figure 11 is consistent with such a transformation. The LUMO of **4** contains significant Sb−Sb and Pt−Sb overlaps. Adding electrons to this orbital would weaken these bonds, the first step in the transformation of **4** into **6**. The platinum atoms then swing away from those antimony atoms but remain attached to the second antimony atom. A lone pair of electrons should form on each Sb atom, and this will be donated to the second rhenium atom, step **b**. The formation of this Re−Sb bond establishes the Re_2Sb_2 core of the structure. Finally, the hydrido ligands shift to terminal positions on the platinum atom, and the Re−Pt bonds are cleaved to complete the formation of cis-**6**.

The formation of trans-**6** is only slightly more complicated in that it requires one additional step, an inversion of configuration at one of the SbPh ligands, see step **d** in Scheme 3. Inversions of the configuration of pyramidal triorganoantimony compounds are known to have energetically high barriers,[24] but this barrier might be lowered if one of the atoms is a 16-electron platinum atom. Finally, the remaining Pt−Re bonds break to complete the formation of trans-**6**, step **e**. Interestingly, we found no evidence for isomerization of cis-**6** to trans-**6** and vice versa when samples of the pure compounds were heated to 100 °C for 5 h. Also, there was no evidence of loss of CO and conversion back to **4** under these conditions. This observation is consistent with the proposed Scheme 3 which shows that trans-**6** is not formed from cis-**6** and vice versa.

Acknowledgment. This research was supported by the National Science Foundation (CHE-0743190 to R.D.A.) and (CHE-0518074, CHE-0541587 and DMS-0216275 to M.B.H.) and the Welch Foundation (A0648 to M.B.H.).

Supporting Information Available: CIF files for each of the structural analyses are available. This material is available free of charge via the Internet at http://pubs.acs.org.

IC801876S

(24) Jacobus, J. *J. Chem. Soc. D* **1971**, 1058–1059.